



\mathcal{PT} -symmetry breaking in a Kitaev chain with one pair of gain-loss potentialsKaustubh S. Agarwal and Yogesh N. Joglekar *Department of Physics, Indiana University–Purdue University Indianapolis, Indianapolis, Indiana 46202, USA* (Received 11 March 2021; revised 13 August 2021; accepted 16 August 2021; published 26 August 2021)

Parity-time (\mathcal{PT}) symmetric systems are classical, gain-loss systems whose dynamics are governed by non-Hermitian Hamiltonians with exceptional-point (EP) degeneracies. The eigenvalues of a \mathcal{PT} -symmetric Hamiltonian change from real to complex conjugates at a critical value of gain-loss strength that is called the \mathcal{PT} breaking threshold. Here, we obtain the \mathcal{PT} threshold for a one-dimensional, finite Kitaev chain—a prototype for a p -wave superconductor—in the presence of a single pair of gain and loss potentials as a function of the superconducting order parameter, on-site potential, and the distance between the gain and loss sites. In addition to a robust, nonlocal threshold, we find a rich phase diagram for the threshold that can be qualitatively understood in terms of the band structure of the Hermitian Kitaev model. In particular, for an even chain with zero on-site potential, we find a re-entrant \mathcal{PT} -symmetric phase bounded by second-order EP contours. Our numerical results are supplemented by analytical calculations for small system sizes.

DOI: [10.1103/PhysRevA.104.022218](https://doi.org/10.1103/PhysRevA.104.022218)**I. INTRODUCTION**

A complex extension to quantum mechanics, based on a special class of non-Hermitian Hamiltonians with purely real spectra, was discovered more than two decades ago [1–4]. These continuum Hamiltonians on an infinite line shared the property that each of them is invariant under combined operations of parity and time-reversal (\mathcal{PT}); i.e., the Hamiltonian commutes with the \mathcal{PT} operator. Over the past decade, it has become clear that \mathcal{PT} -symmetric systems represent open, classical systems with balanced, spatially or temporally separated gain and loss that are represented by complex real-space potentials [5–7].

The spectrum E_α of a \mathcal{PT} -symmetric Hamiltonian $H(\gamma)$ is real at small non-Hermiticities γ and turns into complex-conjugate pairs at large non-Hermiticities. When the spectrum is purely real, we can choose an eigenvector $|\epsilon_\alpha\rangle$ of H to be a simultaneous eigenvector of the antilinear \mathcal{PT} -operator with eigenvalue $+1$. When the spectrum is complex, the \mathcal{PT} operator acting on $|E_\alpha\rangle$ transforms it into the eigenvector with a complex-conjugate eigenvalue, i.e., $\mathcal{PT}|E_\alpha\rangle = |E_\alpha^*\rangle$, where $*$ denotes complex conjugation. The transition from a purely real to a complex-conjugate spectrum occurs when $\gamma = \gamma_{\mathcal{PT}}$, where $\gamma_{\mathcal{PT}}$ is called the \mathcal{PT} -symmetry breaking threshold. At the threshold, the geometric multiplicity of the eigenvalues of the Hamiltonian $H(\gamma_{\mathcal{PT}})$ is smaller than the algebraic multiplicity. Such a Hamiltonian degeneracy is called an exceptional point (EP) degeneracy, where not only do the eigenvalues become degenerate, but the corresponding eigenvectors also coalesce.

In the past decade, \mathcal{PT} -symmetric systems with balanced gain-loss have been realized in classical wave systems including evanescently coupled waveguides [8], fiber loops [9], optical resonators [10,11], electrical circuits [12,13], and mechanical oscillators [14]. However, since the EP degeneracies

also occur for Hamiltonians with mode-selective dissipation, the dynamics of \mathcal{PT} -symmetric Hamiltonians have also been realized in purely lossy classical systems consisting of coupled waveguides, resonators or electrical circuits [15,16], semiclassical systems with ultracold atoms [17], and quantum systems [18–20].

In this paper, we obtain the \mathcal{PT} -breaking threshold in a one-dimensional Kitaev model in the presence of one pair of gain-loss potentials $\pm i\gamma$ located on reflection-symmetric sites. The Kitaev model is a toy model for a topological superconductor with Majorana fermions as excitations. A Majorana fermion is, by construction, its own antiparticle, i.e., it is a fermion constructed from an electron-hole pair. However, we emphasize that the topological nature of these excitations is governed by the single-particle band structure, and is independent of the quantum statistics of particles that generate it. There are a number of studies on topological superconductors with non-Hermitian, \mathcal{PT} -symmetric potentials that preserve the translational invariance of the system [21–29]. In these studies, the gain and loss potentials are distributed throughout the lattice, and their focus is on the fate of the edge states that are characterized by zero energy. A finite Kitaev chain with a pair of \mathcal{PT} -symmetric potentials at its boundaries has also been studied [24–27]. The result is the emergence of an additional pair of edge state with a nonzero energy eigenvalue [26]. In contrast to these studies, we focus here on the variation of the \mathcal{PT} -breaking threshold $\gamma_{\mathcal{PT}}(m_0, N)$ with the location m_0 of the gain potential in a Kitaev chain of size N .

This paper is organized as follows. In Sec. II we describe the Hermitian Kitaev chain along with its symmetry properties, and then we introduce the non-Hermitian perturbation. In Sec. III, we present numerical results for the \mathcal{PT} -symmetry breaking threshold as a function of different parameters of the Hermitian model and the relative location of the gain potential for chains with an even number of sites N . We point out key

differences among the \mathcal{PT} -symmetry breaking thresholds for various settings of the on-site potentials μ and superconducting coupling strengths δ . Corresponding results for a chain with odd N are presented in Sec. IV. In Sec. V we describe a small-system case of $N = 5$ sites, and analytically obtain the dependence of the \mathcal{PT} threshold when the gain-loss potentials are farthest apart and closest together. In Sec. VI, we show that the Kitaev model shows a reentrant \mathcal{PT} -symmetric phase, and we map out its EP contours. Finally, in Sec. VII, we conclude by summarizing the results.

II. TIGHT-BINDING MODEL

The Kitaev model of a one-dimensional, p -wave superconducting chain with N sites and open boundary conditions is described by the following Hermitian Hamiltonian:

$$H_0 = -\mu \sum_{n=1}^N c_n^\dagger c_n - J \sum_{n=1}^{N-1} (c_n^\dagger c_{n+1} + \text{H.c.}) + i\delta \sum_{n=1}^{N-1} (c_n c_{n+1} - \text{H.c.}). \quad (1)$$

Here c_n^\dagger and c_n are fermionic creation and annihilation operators for site n in the chain, μ is the on-site potential, $J > 0$ is the nearest-neighbor hopping strength, and $\delta > 0$ is the amplitude of the (p -wave) superconducting coupling for a Cooper pair that is localized across neighboring sites [30]. The global phase of the superconducting order parameter is fixed at $\pi/2$ to ensure that Eq. (1) is parity-time symmetric, with the parity operator given by $\mathcal{P} : c_n \rightarrow c_{\bar{n}}$, where $\bar{n} = N + 1 - n$ is the mirror-symmetric counterpart of site n and the time-reversal operator is given by complex conjugation, $\mathcal{T} = *$. Note that the second-quantized Hamiltonian (1) does not commute with the total fermion number $\hat{N}_f = \sum_{n=1}^N c_n^\dagger c_n$. Therefore, eigenstates H_0 have an indefinite fermion number. We rewrite Eq. (1) by using the Bogoliubov–de Gennes representation in terms of the operator-vector $\Psi = (c_1, c_1^\dagger, c_2, c_2^\dagger, \dots, c_N, c_N^\dagger)^T$ as $H_0 = \Psi^\dagger H_{\text{BdG}} \Psi$, where the $2N \times 2N$ matrix H_{BdG} in the site-representation is given by

$$H_{\text{BdG}} = -\frac{\mu}{2} \sum_{n=1}^N |n\rangle \langle n| \otimes \sigma_z - \frac{J}{2} \sum_{n=1}^{N-1} (|n\rangle \langle n+1| + |n+1\rangle \langle n|) \otimes \sigma_x + \frac{i\delta}{2} \sum_{n=1}^{N-1} (|n\rangle \langle n+1| - |n+1\rangle \langle n|) \otimes \sigma_x, \quad (2)$$

where σ_x, σ_z are the standard Pauli matrices.

From this point on, we will treat Hamiltonian (2) as a model for a quantum particle hopping on a lattice with $2N$ sites. For a chain with periodic boundary conditions, translational invariance allows us to transform Eq. (2) into block-diagonal momentum-space Hamiltonian $\tilde{H}_{\text{BdG}} = \sum_{k=1}^N h(p_k) |p_k\rangle \langle p_k|$, where $p_k = 2\pi k/N$ are the discrete

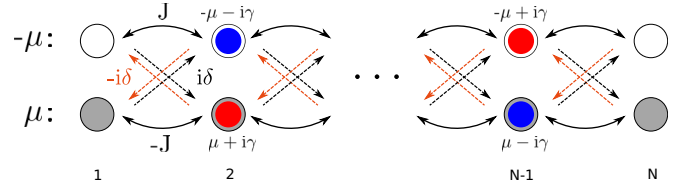


FIG. 1. Schematic representation of a Kitaev model with one pair of gain and loss potentials, Eq. (6). Two chains (gray and white) with on-site potentials $\pm\mu$ have nearest-neighbor Hermitian tunneling amplitudes $\pm J$, and next-nearest-neighbor Hermitian amplitudes $\pm i\delta$. Due to the presence of two rows for each site, the potential $i\gamma$ on site m_0 acts as gain (red) for one and loss (blue) for the other. This schematic can be realized with coupled resonator rings where one can engineer complex, Hermitian tunneling amplitudes [31].

quasimomenta, and

$$h(p) = \begin{pmatrix} -J \cos p - \mu/2 & -i\delta \sin p \\ i\delta \sin p & J \cos p + \mu/2 \end{pmatrix}. \quad (3)$$

The bulk energy spectrum of the Hamiltonian \tilde{H}_{BdG} is given by

$$E_{\pm}(p) = \pm \sqrt{(J \cos p + \mu/2)^2 + \delta^2 \sin^2 p}, \quad (4)$$

and it shows that in the limit of an infinite chain, $N \gg 1$, the gap in the spectrum vanishes at $p = \pi$ when $\mu = 2J$. For the finite chain, the spectrum Eq. (4) is symmetric about $\delta = 0$ because $H_{\text{BdG}}(-\delta) = \mathcal{S} H_{\text{BdG}}(\delta) \mathcal{S}^\dagger$ with a unitary operator $\mathcal{S} = \mathbb{1}_N \otimes \sigma_z$. When the boundary conditions are changed from periodic to open, at $\mu = 0$, excitations localized at the two ends of the chain appear. These edge modes are robust when gain-loss potentials are introduced on random sites [24] or on parity symmetric sites with disorder [26].

To this two-band, single-particle model with open boundary conditions, we add a pair of balanced gain-loss potentials $\pm i\gamma$ at mirror symmetric sites m_0 and \bar{m}_0 ,

$$i\Gamma = \frac{i\gamma}{2} (|m_0\rangle \langle m_0| - |\bar{m}_0\rangle \langle \bar{m}_0|) \otimes \sigma_z, \quad (5)$$

and thereby get a non-Hermitian, \mathcal{PT} -symmetric Kitaev chain Hamiltonian

$$H_{\text{K}}(\gamma, \delta, \mu) = H_{\text{BdG}} + i\Gamma. \quad (6)$$

Note that we do not consider the second-quantized version of Eq. (5), i.e., $i\gamma (c_{m_0}^\dagger c_{m_0} - c_{\bar{m}_0}^\dagger c_{\bar{m}_0})$. Since fermions obey the Pauli principle, their occupation numbers are limited to 0 or 1, and thus gain for the fermion number is not possible. Instead, Hamiltonian (6) represents an effective, two-band model.

Figure 1 shows a schematic representation of a lattice model described by Eq. (6). Although the original model refers to many-body fermionic system with two bands, in its “single-particle” form, Eq. (6) has the following interpretation: It represents two rows, each with N sites. The top (bottom) row has on-site potential $-\mu$ (μ). The nearest-neighbor hopping in the top row is given by $J > 0$, while the bottom row has nearest-neighbor hopping $-J < 0$. There is a Hermitian purely imaginary hopping $\pm i\delta$ that connects site n in the top row to sites $n \pm 1$ in the bottom row. In this representation, the non-Hermitian potential at site m_0 is a loss (gain) for the top (bottom) row, whereas for its reflection-symmetric site \bar{m}_0 , it is a gain (loss) for the top (bottom)

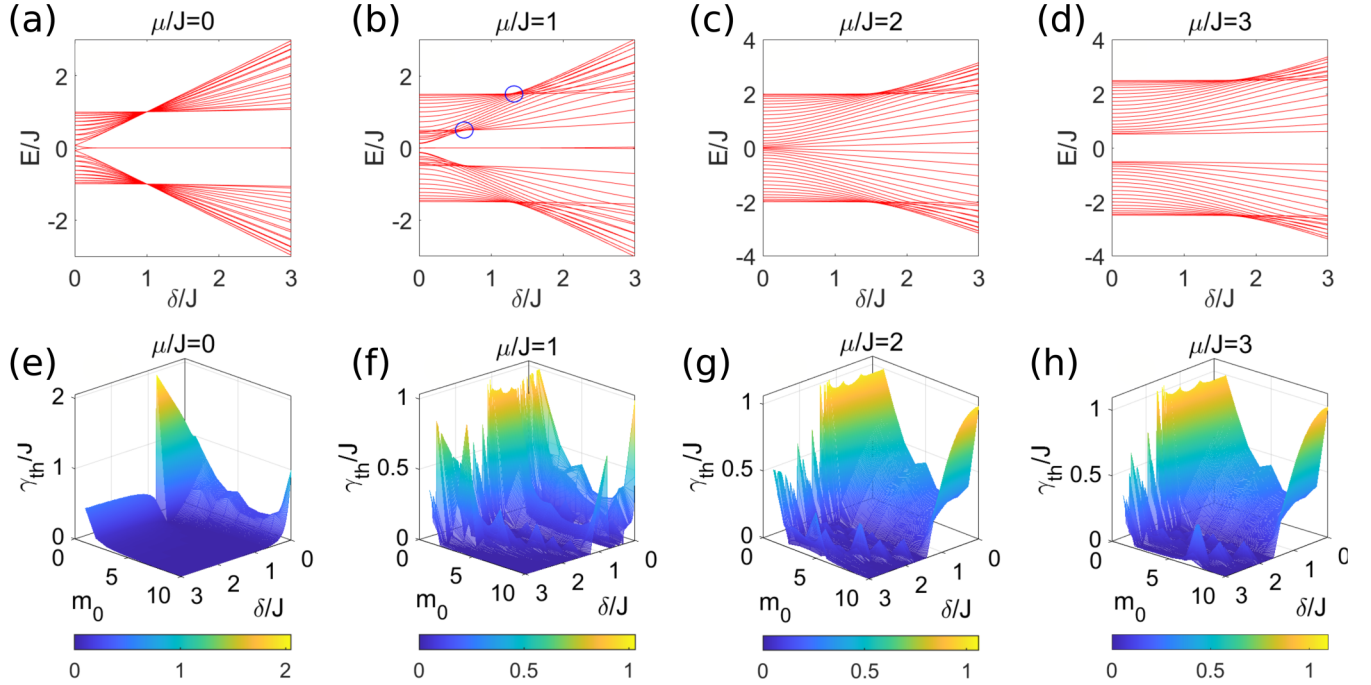


FIG. 2. Energy eigenvalues (in units of J) of an $N = 20$ -site Hamiltonian $H_{\text{BdG}}(\delta)$, Eq. (2), as a function of detuning. (a) $\mu/J = 0$ and (b) $\mu/J = 1$ have topological edge modes, while the system is in the topologically trivial phase at (c) $\mu/J = 2$ and (d) $\mu/J = 3$. Corresponding \mathcal{PT} threshold values γ_{th}/J obtained from the Hamiltonian H_{K} , Eq. (6), are plotted as a function of the gain location $m_0 \in [1, N/2]$ and the superconducting order parameter δ/J : (e) $\mu/J = 0$, (f) $\mu/J = 1$, (g) $\mu/J = 2$, and (h) $\mu/J = 3$. Most of these features can be understood in terms of Hermitian band structure (a)–(d). The spiky structure of the $\gamma_{\text{th}}(m_0, \delta)$ manifold in (e)–(h) is due to finite-size effects.

row. This representation of the \mathcal{PT} -symmetric Kitaev model, with complex tunneling amplitudes and gain-loss potentials, can be experimentally implemented in resonator arrays with off-center links [31]. Alternatively, the Hamiltonian (6) also denotes a quantum particle with local (pseudospin) degree of freedom hopping on an N -site lattice [32]. In the next section, we explore the global phase diagram for the \mathcal{PT} -symmetry breaking threshold $\gamma_{\text{th}}(m_0, \delta, \mu)$.

III. THRESHOLD BEHAVIOR FOR AN EVEN CHAIN

The results presented in this section are obtained by diagonalizing H_{K} or H_{BdG} for Kitaev chains with even system size, i.e., $N = 20$ (Fig. 2). They remain qualitatively the same for larger chain sizes, and the differences between even- and odd-parity chains persist in the large- N limit, as they do for a simple tight-binding model [33]. All energies are measured in units of the tight-binding coupling $J = 1$.

Figures 2(a)–2(d) show the energy eigenvalues E_n for a Hermitian Kitaev chain as a function of the superconducting order parameter δ/J . When $\delta = 0 = \mu$, we get the doubly degenerate cosine-band of a tight-binding model. As the detuning δ is increased from (a) to (d), the two bands become well-separated. On the other hand, at a fixed detuning, when δ is increased, the bands develop fanlike linear dispersion, leading to massively degenerate flat bands at $\delta/J = 1$ at zero detuning. As the detuning is increased from $\mu = 0$, the system develops two crossing points [shown by blue circles in (b)]. We also note that doubly degenerate zero-energy states are present when $\mu < 2J$. At $\mu = 0$, these topological, edge-localized states are fully localized on the end sites. When μ

is increased, these states extend into the bulk of the chain, with an exponentially decaying probability density [28,29]. At $\mu/J = 2$, the superconducting gap closes, marking a phase transition to the topologically trivial phase, Fig. 2(c). Here the midgap states become a part of the bulk. When μ is increased further, Fig. 2(d), the system is in the trivial superconducting phase, and the energy spectrum is gapped.

Generically, \mathcal{PT} -symmetry breaking occurs when two (or more) adjacent levels of the Hermitian Hamiltonian are connected by the gain-loss potential. This introduces level-attraction leading to an exceptional-point degeneracy [34]. For a tight-binding chain, most eigenstates of the Hermitian Hamiltonian are extended in real space. Therefore, a single gain-loss pair, on reflection-symmetric sites, will connect all adjacent levels to each other, except for the levels whose wave functions have a node at the gain (and, due to reflection-symmetric eigenfunctions, loss) sites. Thus, the \mathcal{PT} -symmetry breaking threshold is determined by the smallest gap in the Hermitian band structure [35]. In other words, the Hermitian (near or exact) degeneracies of the Hamiltonian H_{BdG} play an important role in determining the threshold gain-loss strength γ_{th} when a pair of gain-loss potentials is introduced at mirror symmetric sites.

Figures 2(e)–2(h) show the numerically determined \mathcal{PT} -symmetry breaking threshold γ_{th} for the $N = 20$ chain as a function of m_0 and superconducting order parameter δ . When $\mu/J = 0$ [panel (e)], we see that $\gamma_{\text{th}}(m_0, \delta)$ has the characteristic U-shaped behavior [33] when $\delta = 0$ and becomes mostly zero for intermediate locations $m_0 \sim N/4$. When $m_0 = 1$, i.e., when the gain-loss locations are farthest apart, the \mathcal{PT} threshold is maximized to $\gamma_{\text{th}} = J$, and reflects the nonlocal

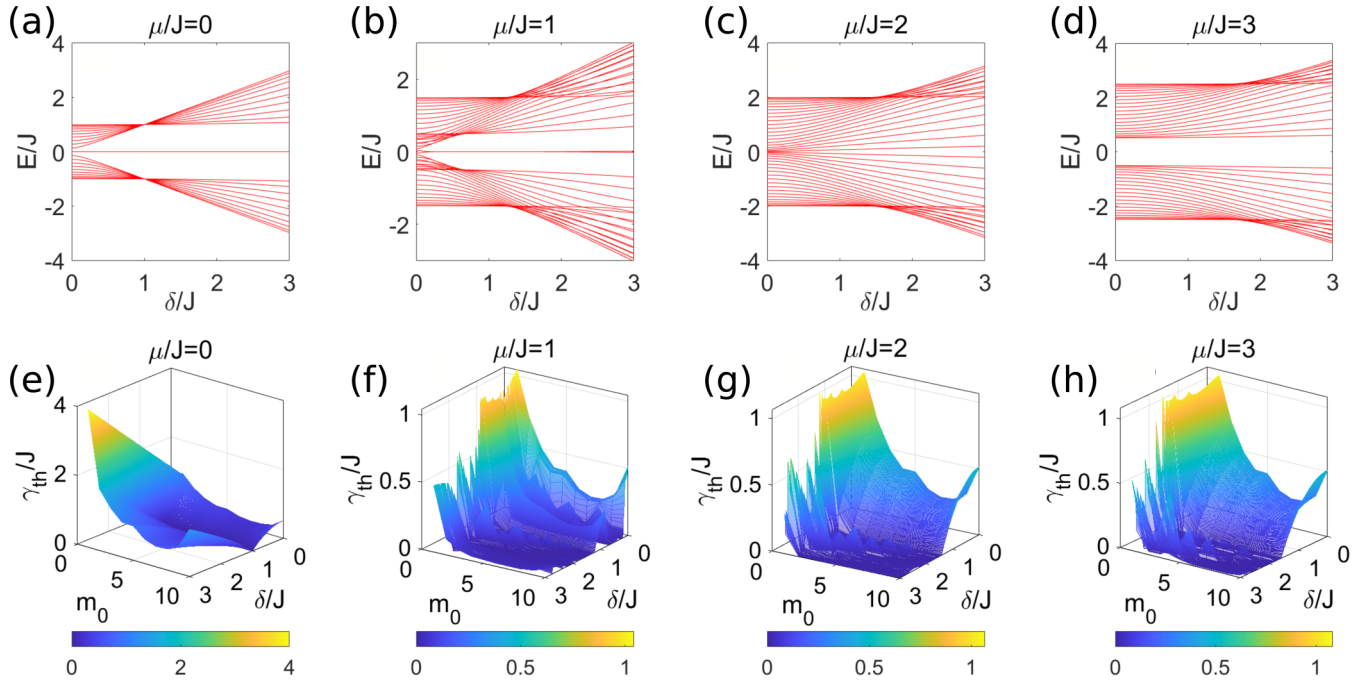


FIG. 3. Energy eigenvalues (in units of J) of an $N = 21$ -site Hamiltonian $H_{\text{BdG}}(\delta)$, Eq. (2), as a function of detuning. (a) $\mu/J = 0$ and (b) $\mu/J = 1$ have midgap states with zero energy, but these are not topological. (c) $\mu/J = 2$ and (d) $\mu/J = 3$ show the emergence of a gapped spectrum. Corresponding \mathcal{PT} threshold values γ_{th}/J obtained from the Hamiltonian H_{K} , Eq. (6), are plotted as a function of the gain location $m_0 \in [1, (N-1)/2]$ and the superconducting order parameter δ/J : (e) $\mu/J = 0$, (f) $\mu/J = 1$, (g) $\mu/J = 2$, (h) $\mu/J = 3$. Due to the absence of topological edge modes, the \mathcal{PT} threshold behavior at $\mu = 0$ is markedly different from that of an even chain, Fig. 2(e). At nonzero detuning, the threshold is nonmonotonically suppressed with increasing δ . The spiky structure of the $\gamma_{\text{th}}(m_0, \delta)$ manifold in (e)–(h) is due to finite-size effects.

robustness that is ubiquitous for systems with open boundary conditions [33,36]. In this case, the states that participate in the \mathcal{PT} -breaking process are the midband states. As m_0 is increased, the threshold decreases and it rises back to $\gamma_{\text{th}} = J$ when the gain and loss locations are nearest neighbors, i.e., $m_0 = N/2$. In this situation, all eigenvalues simultaneously and pairwise become complex, giving rise to maximal \mathcal{PT} -symmetry breaking [37].

Next, we focus on the variation of the threshold with the superconducting order parameter δ . In contrast to the variation with m_0 , the \mathcal{PT} -threshold is uniformly suppressed from its $\delta = 0$ value for most gain-loss locations. The exception is the region $m_0 \sim 1$, where, as δ is increased, we see that the \mathcal{PT} threshold at $\delta = J$ rises to double its $\delta = 0$ value [26], where the flat bands occur; see Fig. 2(a). As δ is increased further, the threshold dips to zero and then increases, reaching a steady, δ -independent value of $\gamma_{\text{th}} = J/2$. As the detuning μ is increased from zero, Fig. 2(f), there is an overall suppression of the \mathcal{PT} -breaking threshold γ_{th} , although the characteristic U-shape behavior as a function of m_0 and the nonmonotonic behavior as a function of δ for farthest gain-loss potentials are both retained. These qualitative trends continue for $\mu \leq 2J$.

When the detuning is large, $\mu > 2J$, the system enters a trivial superconducting phase with no edge localized states, (g) and (h). In this regime, the system consists of two separated bands, and therefore the \mathcal{PT} -threshold does not sensitively depend on the detuning. On the other hand, when gain and loss are on nearest-neighbor sites, $m_0 = N/2$, the threshold is suppressed to zero for $\delta \sim 2J$. This is explained by the

level crossings that occur at the band edges; see Figs. 2(c) and 2(d). We note that the spiky structure of the $\gamma_{\text{th}}(m_0, \delta)$ manifold in Figs. 2(e)–2(h) is due to finite-size effects. In the thermodynamic limit, $N \rightarrow \infty$, the threshold algebraically vanishes except for when the gain-loss potentials are farthest away ($m_0 = 1$) or closest to each other ($m_0 = N/2$) [33].

Lastly, we comment on the degree of exceptional point (EP) accompanying the \mathcal{PT} -symmetry breaking transition. For even N , we have zero-energy, topological states only when $\mu = 0$ and $\delta = 1$. These states, along with two particle-hole symmetric states, participate in the \mathcal{PT} -breaking transition only when $m_0 = 1$. Therefore, except in this case, the \mathcal{PT} -transition occurs via a second-order exceptional point (EP2).

IV. THRESHOLD BEHAVIOR FOR AN ODD CHAIN

Are there any differences in the threshold behavior for an odd Kitaev chain? Figure 3 shows corresponding, representative results for a chain with $N = 21$ sites. Panels (a)–(d) show the dispersions of the Hermitian Kitaev chain as a function of δ/J for increasing detuning values. At zero detuning, panel (a), the band structure looks similar to that in Fig. 2(a). As μ is increased, the qualitative evolution of the band structure is similar to that of an even Kitaev chain, with the band gap closing at $\mu = 2J$ and well-separated two-band structure at higher detuning values. The key difference with the even N chain is that there is no degenerate pair of topological zero-energy states when N is odd. This absence leads to dramatically different behavior for the \mathcal{PT} -symmetric breaking threshold

at zero detuning $\mu = 0$. The numerically obtained threshold γ_{th}/J manifolds are shown in the m_0 - δ/J plane as a function of detuning μ in Figs. 3(e)–3(h).

Panel (e) shows the results at zero detuning, $\mu = 0$. Near $\delta = 0$ —no superconducting term—we recover the characteristic U-shaped dependence with a robust threshold $\gamma_{\text{th}} \sim J$ when $m_0 = 1$, i.e., the farthest gain and loss pairs. In contrast, for the closest gain-loss locations, i.e., $m_0 = (N - 1)/2$, the threshold reaches $\gamma_{\text{th}} \sim J/2$ [33,35,37]. On the other hand, the behavior of the threshold γ_{th} as a function of δ is markedly different from corresponding results for an even chain [Fig. 2(e)]. When $m_0 = 1$, for an even N the threshold γ_{th} first rises to $2J$, then dips to zero at $\delta/J = 1$, and then flattens asymptotically to $\gamma_{\text{th}} = J/2$.

For an odd chain, however, the threshold monotonically increases as δ is increased. When $m_0 = 1$, particle-hole symmetric states (at the bottom of the top band and the top of the bottom band) coalesce with the nontopological zero-energy state, giving rise to an EP3 [33]. Since level separation between the particle-hole symmetric states increases monotonically with δ , Fig. 3(a), the \mathcal{PT} -symmetry breaking threshold increases as well. This is true even at $\delta = 1$, when the system develops flat bands—recall that for an even chain, the threshold γ_{th} is zero, $\delta = 1$. As γ is increased, two degenerate states from the top-flat-band (along with their particle-hole counterpart states) flow towards the zero-energy states. Thus, for an odd chain, the \mathcal{PT} -breaking transition occurs across an EP3 for all values of δ , as long as the chain is at zero detuning ($\mu = 0$) and $m_0 = 1$.

Compared to the results at zero detuning, Fig. 3(e), the behavior of the threshold γ_{th}/J at finite detuning is markedly different; see Figs. 3(f)–3(h). The threshold shows a non-monotonic suppression of γ_{th} with increasing δ/J . These results at finite μ bear close resemblance to corresponding results for an even chain, Figs. 2(f)–2(h). Just as in the even N case, the spiky structures in the $\gamma_{\text{th}}(m_0, \delta)$ manifold are finite-size effects; they are also relevant because in experiments, coupled waveguide or resonator lattices are usually limited to $N \lesssim 20 - 30$.

Lastly, we point out the effect of topological edge states on the \mathcal{PT} -threshold. The even- N lattice supports edge-localized, midgap, robust, topological states when $m\mu/J \leq 2$. In contrast, for odd N , there are no topological midgap states. These states are primarily coupled to the gain-loss potentials when they are at edges, i.e., $m_0 = 1$. The difference between the coupling to a topological state versus a nontopological state is manifest in the threshold $\gamma_{\text{th}}(m_0 = 1)$, which shows dramatically different behavior as a function of superconducting order parameter δ/J ; see Figs. 2(e) and 3(e).

V. ANALYTICAL APPROACH

From the numerical results, we see that a nonzero \mathcal{PT} threshold emerges in the thermodynamic limit only when the gain-loss pairs are either at the end of the chain ($m_0 = 1$) or closest to one other [$m_0 = N/2$ or $m_0 = (N - 1)/2$]. To understand the global behavior of the \mathcal{PT} threshold $\gamma_{\text{th}}(m_0, \mu, \delta)$ in an odd chain, we look towards the smallest nontrivial case with zero detuning, i.e., $N = 5$ and $\mu = 0$.

When $m_0 = 1$, the doubly degenerate, particle-hole symmetric spectrum is analytically tractable. The eight eigenvalues are given by

$$E_n = \frac{\mp 1}{2\sqrt{2}} [4(J^2 + \delta^2) - \gamma^2 \pm \sqrt{4(J^2 - \delta^2)^2 + \gamma^4}]^{1/2}, \quad (7)$$

along with two (degenerate) zero eigenvalues, $E_{5,6} = 0$. As γ is increased, the energy levels $E_{3,4} = -E_{7,8}$ first approach each other, merge with the zero levels, and then become complex conjugate, thereby giving rise to an exceptional point of order 3 (EP3). The \mathcal{PT} -threshold in this case is given by

$$\gamma_{\text{th}}(m_0 = 1) = J \left[\frac{3(\delta^2 + J^2)^2 + 4\delta^2 J^2}{2J^2(\delta^2 + J^2)} \right]^{1/2}. \quad (8)$$

When $\delta = 0$, the threshold reduces to the uniform tight-binding chain result [37]. In the other limit, $\delta/J \gg 1$, the threshold shows a linear behavior $\gamma_{\text{th}} = \sqrt{3/2}\delta$ that is seen in Fig. 3(e).

When $m_0 = 2$, i.e., the gain and loss locations are closest to each other, the doubly degenerate, particle-hole symmetric eigenvalues are given by

$$E_n = \frac{\mp 1}{2\sqrt{2}} [4(J^2 + \delta^2) - \gamma^2 \pm \sqrt{A}]^{1/2}, \quad (9)$$

$$A = 4(J^2 - \delta^2)^2 + \gamma^4 - 8\gamma^2(J^2 + \delta^2), \quad (10)$$

along with two (degenerate) zero eigenvalues, $E_{5,6} = 0$. As γ is increased, the levels near the band-edge approach each other and become degenerate, giving rise to an EP2. The \mathcal{PT} threshold, obtained by requiring $E_{1,2}(\gamma_{\text{th}}) = E_{3,4}(\gamma_{\text{th}})$ or equivalently $A(\gamma_{\text{th}}) = 0$, is given by

$$\gamma_{\text{th}}(m_0 = 2) = (J^2 + \delta^2) - 2\sqrt{3(\delta^2 + J^2)^2 + 4\delta^2 J^2}^{1/2}. \quad (11)$$

When $\delta = 0$, the threshold reduces to the uniform tight-binding result. On the other hand, when $\delta/J \gg 1$, the threshold shows a linear behavior $\gamma_{\text{th}} = \sqrt{2}\delta$. We note that for this small- N case, the threshold does not reduce to zero at $\delta = 1$. These analytical results are only valid for zero detuning; for finite detuning $\mu > 0$ we have to resort to numerical calculations.

Figure 4(a) shows the schematic of a five-site chain with gain-loss potentials at its ends, i.e., $m_0 = 1$. Panels (b) and (c) show the flow of the real parts of energy eigenvalues for the model as a function of γ/J for different values of δ . We see that increasing γ leads to \mathcal{PT} -breaking that occurs at the center of the band, giving rise to an EP3. They also show that the threshold increases monotonically with δ , consistent with what is seen in Fig. 3(e). Panel (d) shows a numerically obtained threshold diagram in the μ - δ plane.

Figure 4(e) shows the configuration with nearest-possible gain-loss potentials, i.e., $m_0 = 2$. Panels (f) and (g) show the flow of the real part of eigenvalues for the model. Increasing γ in this case leads to \mathcal{PT} -breaking at the band edges, and it has a nonmonotonic dependence on the superconducting order parameter δ , also seen in Fig. 3(e). Panel (h) shows numerically obtained threshold $\gamma_{\text{th}}(\mu, \delta)$. We will see below that this beak-shaped threshold map in the μ - δ plane is generic.

Figure 5 shows the behavior of γ_{th}/J for nearest-neighbor gain-loss potentials, $m_0 = N/2$, as a function of μ/J and δ/J

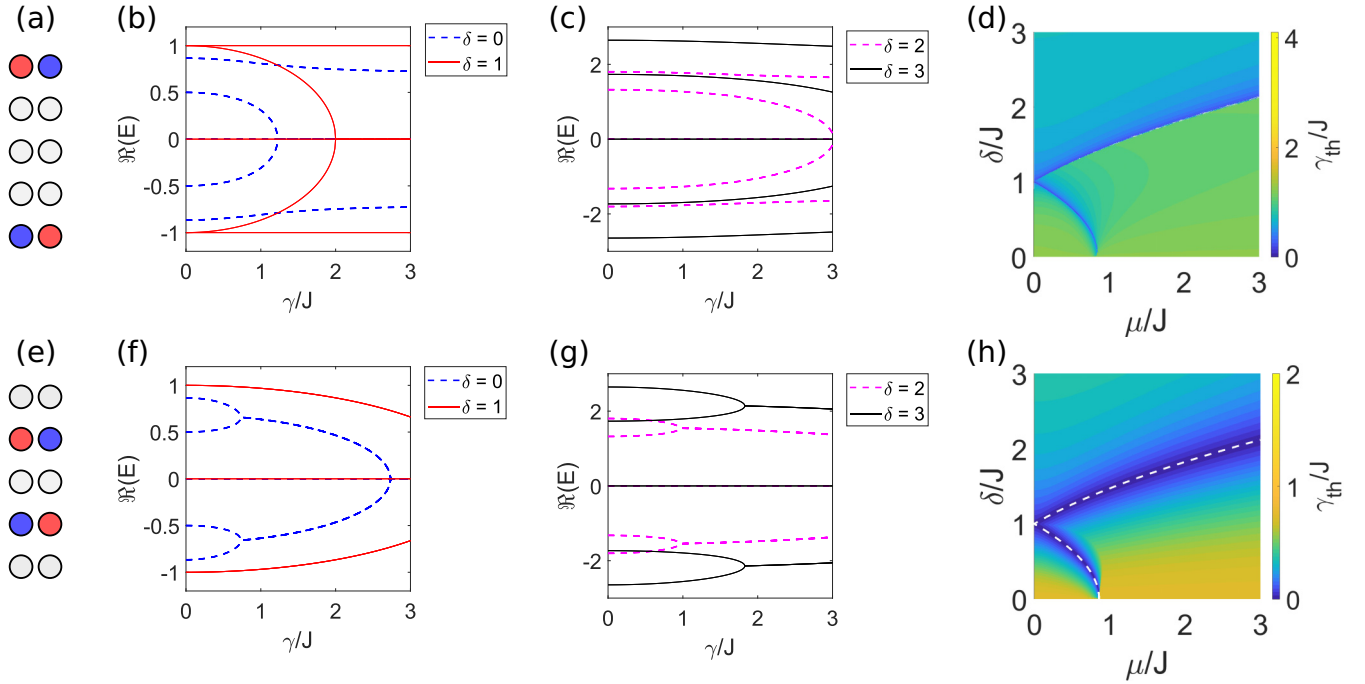


FIG. 4. \mathcal{PT} threshold for an $N = 5$ chain. (a) Schematic of an $N = 5$ chain with $m_0 = 1$. (b), (c) Flow of the real part of eigenvalues of the $N = 5$ chain as a function of γ for the farthest gain-loss locations (far left) shows that \mathcal{PT} breaking occurs at an EP3 and the threshold increases monotonically with the superconducting order parameter δ . (d) $\gamma_{\text{th}}(\mu, \delta)$ shows a beak-shaped pattern including a contour of zero threshold given by $\alpha\mu J + |J^2 - \delta^2| = 0$. (e) Schematic of $N = 5$ chain with $m_0 = 2$. (f), (g) Corresponding results for closest gain-loss locations, $m_0 = 2$, show that \mathcal{PT} -breaking occurs at an EP2, and the threshold varies nonmonotonically with δ . (h) $\gamma_{\text{th}}(\mu, \delta)$ map shows features similar to those in panel (d). The white-dashed line is the zero-threshold contour given by $\alpha\mu J + |J^2 - \delta^2| = 0$ with $\alpha = 1.6$.

for an $N = 20$ -site chain. Apart from the nonzero threshold that occurs in the limit $\delta = 0$ for any detuning, we see that $\gamma_{\text{th}} = 0$ for large δ for any μ , and there is a beak-shaped region in the μ - δ plane with a positive \mathcal{PT} threshold. In the magnified view of the region at small $\delta/J < 1$ [Fig. 5(b)], we see significant variations in the \mathcal{PT} threshold as we sweep across μ/J . These threshold “dips” occur at values of μ/J where the lowest energy levels in the bulk become degenerate. The white dashed line in Fig. 5(a), separating the zero-threshold region from the positive-threshold regions, is described by equation $\alpha\mu J + |J^2 - \delta^2|$, where $\alpha \sim 0.5$ is an N -dependent constant. The region $0 < \mu/J < 2$, $0 < \delta/J < 1$ enveloped in the \mathcal{PT} phase boundary shows many ripples with $\gamma_{\text{th}} > 0$. These ripples are finite-size effects that vanish in the thermodynamic limit $N \rightarrow \infty$.

We remind the reader that in the current configuration, $m_0 = N/2$, only the states near the band edges become degenerate and then complex-conjugate. To find the asymptotic behavior of the zero-threshold line, we turn to the Hermitian band structure, Eq. (4). A zero threshold is a result of degeneracy in the consecutive levels, i.e., $E(q_k) = E(q_{k-1})$, where $q_k = \pi k/(N+1)$ are the lattice quasimomenta consistent with open boundary conditions. Simplifying the degeneracy criterion gives

$$a_1\mu J + a_2(J^2 - \delta^2) = 0, \quad (12)$$

$$a_1 = \cos(q_k) - \cos(q_{k-1}), \quad (13)$$

$$a_2 = a_1[\cos(q_k) + \cos(q_{k-1})]. \quad (14)$$

Defining $\alpha = a_1/|a_2|$, we obtain an analytical expression for the asymptotic value of α . From the energy spectra in Figs. 2(a)–2(d) and numerical analysis, it follows that regions near $q \sim 0, \pi$ contribute giving $\alpha \rightarrow 0.5$ in the limit $N \rightarrow \infty$. At the other limit, when $N = 5$ fitting the zero threshold contour to the form $\alpha\mu J + |J^2 - \delta^2| = 0$ [dashed white line in Fig. 4(h)], we obtain $\alpha = 1.6$.

VI. EXCEPTIONAL LINES AND REENRANT \mathcal{PT} PHASE

In one-dimensional lattice models with a single pair of gain and loss potentially, typically, the \mathcal{PT} -symmetry breaking occurs monotonically with increasing gain-loss strength γ . This is true for uniform chains with open [33] or periodic boundary conditions [38]; the Su-Schrieffer-Heeger, the Aubrey-Andre-Harper or quasiperiodic models [39,40]; and models with nonuniform, parity-time symmetric tunneling profiles [41], including the perfect-state transfer models. On the other hand, the presence of two or more gain-loss potentials can lead to reentrant \mathcal{PT} -symmetric phase [42,43] where increasing gain-loss strength leads to repeated \mathcal{PT} -symmetry breaking and \mathcal{PT} -symmetry restoration transitions.

In contrast to these models with multiple non-Hermitian terms [42,43], the Kitaev chain we have considered shows a reentrant \mathcal{PT} -symmetric phase and its subsequent breaking when the gain-loss strength γ is increased. This phenomenon occurs for an even chain with $\mu = 0$ and $m_0 = 1$, at moderate superconducting order parameter $1 \leq \delta/J \leq \sqrt{2}$, independent of the chain size. In Fig. 6(a), we plot $\Lambda(\gamma, \delta) = \log_{10} \max_k \text{Im}(E_k)$, where E_k are (purely real or

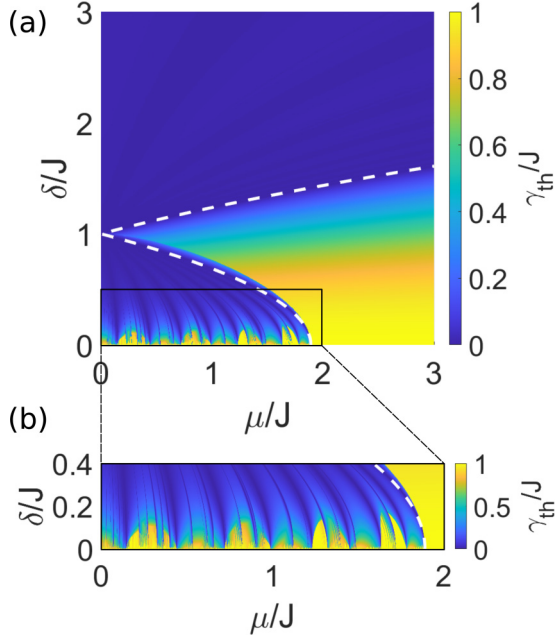


FIG. 5. (a) \mathcal{PT} -symmetry threshold for a chain with $N = 20$ and $m_0 = N/2$. The white dashed line, separating the zero-threshold region from the nonzero-threshold region, is empirically fit by the equation $\alpha\mu J + |J^2 - \delta^2| = 0$, where $\alpha \rightarrow 0.5$ as $N \rightarrow \infty$; at $N = 20$, we find that $\alpha = 0.53$. This functional dependence can be obtained by requiring that two adjacent levels in the Hermitian band-structure become degenerate to get $\gamma_{\text{th}} = 0$. (b) Closeup of the boxed region near the origin shows multiple ripples in γ_{th} . They are finite-size effects.

complex-conjugate) eigenvalues of the Hamiltonian H_K for an $N = 8$ chain. The \mathcal{PT} -symmetric region is marked by black, and the rest is the \mathcal{PT} -symmetry broken region. With $\delta/J \sim 1$, as γ is increased, the first \mathcal{PT} -symmetry breaking near $\gamma/J \sim 0.5$ occurs due to the level-attraction between and coalescence of two highest energy states in the upper band; recall that due to the particle-hole symmetric nature of the spectrum, two lowest energy levels in the lower band concurrently become degenerate. When γ is increased further while the system is in the \mathcal{PT} -symmetry broken region, subsequent lower energy levels, except the lowest state in the upper band, coalesce in pairs. This sequence of transitions occurs at exceptional points in the \mathcal{PT} -symmetry broken region. Further increasing γ leads to a reverse process where levels with complex-conjugate energies undergo level-attraction and \mathcal{PT} -symmetry is restored. For the lowest-energy states in the upper band (and their chiral counterparts), the reentrant \mathcal{PT} -symmetric phase is accompanied by a qualitative change where the wave-function weight shifts from the bulk to the edges. As γ is increased further, the system enters the \mathcal{PT} -broken region again. This second \mathcal{PT} transition across an EP is driven by coalescence of the near-zero-energy state with the state at the bottom of the top band.

To map out the EP contours numerically in the δ - γ plane, we use the (Dirac) inner-product matrix $M_{pq} = |\langle \psi_p | \psi_q \rangle| \geq 0$, where $|\psi_k\rangle$ is the (Dirac)-normalized right eigenvector of H_K with eigenvalue λ_k . Note that the off-diagonal entries of the inner-product matrix are bounded by 1, i.e., $M_{p \neq q} \leq 1$. This

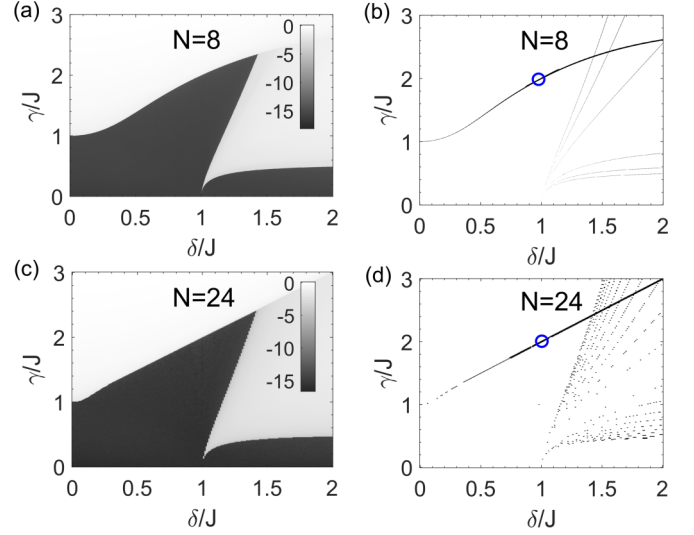


FIG. 6. (a) \mathcal{PT} phase diagram in the γ - δ plane for an $N = 8$ lattice with $\mu = 0$ and $m_0 = 1$ shows the heat map of $\Lambda \equiv \log_{10} \max_k \text{Im}(E_k)$, where E_k are the $2N$ eigenvalues of H_K , Eq. (6). A reentrant \mathcal{PT} -symmetric phase (black) emerges in the range $1 \leq \delta/J \leq \sqrt{2}$ as the gain-loss strength γ/J is increased. (b) EP2 contours at the \mathcal{PT} boundary and in the \mathcal{PT} -broken region show sequential coalescence of eigenvalues. At $\delta/J = 1$, due to the presence of robust Majorana modes, a third-order EP emerges at $\gamma/J = 2$ (blue circle). (c), (d) Corresponding results for an $N = 24$ lattice show the same qualitative features.

bound is saturated if and only if two (or more) eigenvectors of H_K coalesce. Thus EPs are determined by the constraint $M_{p \neq q} = 1$, and their order is given by $\max_p \sum_{q \neq p} M_{pq}$ since that counts the number of eigenvectors that coalesce together. Figure 6(b) shows numerically obtained EP contours. In addition to the boundaries of \mathcal{PT} -symmetric and \mathcal{PT} -broken regions, seen in Fig. 6(a), we see EP contours that denote the cascades of eigenvalue coalescence that occur in the \mathcal{PT} -broken region as γ is increased. Of particular interest is the contour that starts at $\delta = 0$ and $\gamma/J = 1$. At point $\delta/J = 1$, the system has fully degenerate bands with robust, midgap edge states [Fig. 2(a)]. Therefore, introduction of the gain-loss potentials leads to a third-order EP at $\gamma/J = 2$ (shown by a blue circle) in the otherwise second-order EP contour. We note that the prominent reentrant \mathcal{PT} phases only occur when the gain-loss potentials are farthest apart, i.e., $m_0 = 1$, and remain robust only at $\mu = 0$ for any even N ; Figs. 6(c) and 6(d) show that the phase diagram and EP contours for a larger Kitaev chain, $N = 24$, remain qualitatively the same.

VII. CONCLUSION

In this paper, we have investigated the dependence of the \mathcal{PT} -threshold γ_{th} on the properties of the underlying Hermitian Kitaev model and gain-loss potential locations. We have shown that the threshold profile is rich, with persistent differences between even- and odd-parity lattices. In particular, we have found that for a zero-detuning chain with an odd number of sites, the threshold is enhanced with increasing superconducting order parameter. For an even chain with edge

gain-loss potentials and superconducting coupling $\delta \gtrsim 1$, we discover the reentrant \mathcal{PT} -symmetric phase, and \mathcal{PT} -phase boundaries that contain both second- and third-order EPs. We have also discussed, briefly, a potential realization of

our lattice model with coupled optical resonators. Our results further the understanding of non-Hermitian condensed-matter models in the presence of realistically achievable gain and loss.

-
- [1] C. M. Bender and S. Boettcher, *Phys. Rev. Lett.* **80**, 5243 (1998).
- [2] C. M. Bender, D. C. Brody, and H. F. Jones, *Phys. Rev. Lett.* **89**, 270401 (2002).
- [3] A. Mostafazadeh, *J. Math. Phys.* **43**, 205 (2002).
- [4] A. Mostafazadeh, *Int. J. Geom. Methods Mod. Phys.* **07**, 1191 (2010).
- [5] L. Feng, R. El-Ganainy, and L. Ge, *Nat. Photon.* **11**, 752 (2017).
- [6] R. El-Ganainy, K. G. Makris, M. Khajavikhan, Z. H. Musslimani, S. Rotter, and D. N. Christodoulides, *Nat. Phys.* **14**, 11 (2018).
- [7] Ş. K. Özdemir, S. Rotter, F. Nori, and L. Yang, *Nat. Mater.* **18**, 783 (2019).
- [8] C. E. Rüter, K. G. Makris, R. El-Ganainy, D. N. Christodoulides, M. Segev, and D. Kip, *Nat. Phys.* **6**, 192 (2010).
- [9] A. Regensburger, C. Bersch, M.-A. Miri, G. Onishchukov, D. N. Christodoulides, and U. Peschel, *Nature* **488**, 167 (2012).
- [10] L. Chang, X. Jiang, S. Hua, C. Yang, J. Wen, L. Jiang, G. Li, G. Wang, and M. Xiao, *Nat. Photon.* **8**, 524 (2014).
- [11] H. Hodaei, M.-A. Miri, M. Heinrich, D. N. Christodoulides, and M. Khajavikhan, *Science* **346**, 975 (2014).
- [12] J. Schindler, A. Li, M. C. Zheng, F. M. Ellis, and T. Kottos, *Phys. Rev. A* **84**, 040101(R) (2011).
- [13] Y. Choi, C. Hahn, J. W. Yoon, and S. H. Song, *Nat. Commun.* **9**, 2182 (2018).
- [14] C. M. Bender, B. K. Berntson, D. Parker, and E. Samuel, *Am. J. Phys.* **81**, 173 (2013).
- [15] A. Guo, G. J. Salamo, D. Duchesne, R. Morandotti, M. Volatier-Ravat, V. Aimez, G. A. Siviloglou, and D. N. Christodoulides, *Phys. Rev. Lett.* **103**, 093902 (2009).
- [16] R. d. J. Leon-Montiel, M. A. Quiroz-Juarez, J. L. Dominguez-Juarez, R. Quintero-Torres, J. L. Aragon, A. K. Harter, and Y. N. Joglekar, *Commun. Phys.* **1**, 88 (2018).
- [17] J. Li, A. K. Harter, J. Liu, L. de Melo, Y. N. Joglekar, and L. Luo, *Nat. Commun.* **10**, 855 (2019).
- [18] Y. Wu, W. Liu, J. Geng, X. Song, X. Ye, C.-K. Duan, X. Rong, and J. Du, *Science* **364**, 878 (2019).
- [19] M. Naghiloo, M. Abbasi, Y. N. Joglekar, and K. W. Murch, *Nat. Phys.* **15**, 1232 (2019).
- [20] F. Klauck, L. Teuber, M. Ornigotti, M. Heinrich, S. Scheel, and A. Szameit, *Nat. Photon.* **13**, 883 (2019).
- [21] X. Wang, T. Liu, Y. Xiong, and P. Tong, *Phys. Rev. A* **92**, 012116 (2015).
- [22] C. Li, X. Z. Zhang, G. Zhang, and Z. Song, *Phys. Rev. B* **97**, 115436 (2018).
- [23] S. Yao and Z. Wang, *Phys. Rev. Lett.* **121**, 086803 (2018).
- [24] C. Yuce, *Phys. Rev. A* **93**, 062130 (2016).
- [25] M. Klett, H. Cartarius, D. Dast, J. Main, and G. Wunner, *Phys. Rev. A* **95**, 053626 (2017).
- [26] K. Kawabata, Y. Ashida, H. Katsura, and M. Ueda, *Phys. Rev. B* **98**, 085116 (2018).
- [27] C. Li, L. Jin, and Z. Song, *Sci. Rep.* **10**, 6807 (2020).
- [28] S. D. Sarma, M. Freedman, and C. Nayak, *npj Quantum Inf.* **1**, 15001 (2015).
- [29] N. Leumer, M. Marganska, B. Muralidharan, and M. Grifoni, *J. Phys.: Condens. Matter* **32**, 445502 (2020).
- [30] A. Y. Kitaev, *Phys. Usp.* **44**, 131 (2001).
- [31] M. Hafezi, E. A. Demler, M. D. Lukin, and J. M. Taylor, *Nat. Phys.* **7**, 907 (2011).
- [32] H. Vemuri and Y. N. Joglekar, *Phys. Rev. A* **87**, 044101 (2013).
- [33] Y. N. Joglekar, D. Scott, M. Babbey, and A. Saxena, *Phys. Rev. A* **82**, 030103(R) (2010).
- [34] S. Klaiman, U. Günther, and N. Moiseyev, *Phys. Rev. Lett.* **101**, 080402 (2008).
- [35] K. S. Agarwal, R. K. Pathak, and Y. N. Joglekar, *Phys. Rev. A* **97**, 042107 (2018).
- [36] Y. N. Joglekar, C. Thompson, D. D. Scott, and G. Vemuri, *Eur. Phys. J. Appl. Phys.* **63**, 30001 (2013).
- [37] Y. N. Joglekar and J. L. Barnett, *Phys. Rev. A* **84**, 024103 (2011).
- [38] D. D. Scott and Y. N. Joglekar, *Phys. Rev. A* **85**, 062105 (2012).
- [39] A. K. Harter, T. E. Lee, and Y. N. Joglekar, *Phys. Rev. A* **93**, 062101 (2016).
- [40] A. K. Harter, F. A. Onanga, and Y. N. Joglekar, *Sci. Rep.* **8**, 44 (2018).
- [41] Y. N. Joglekar, C. Thompson, and G. Vemuri, *Phys. Rev. A* **83**, 063817 (2011).
- [42] Y. N. Joglekar and B. Bagchi, *J. Phys. A* **45**, 402001 (2012).
- [43] C. H. Liang, D. D. Scott, and Y. N. Joglekar, *Phys. Rev. A* **89**, 030102(R) (2014).